Rock and Soil Mechanics

Volume 42 | Issue 7 Article 5

11-23-2021

A constitutive model considering post-liquefaction deformation based on the logarithmic skeleton curve

Qing DONG
College of Transportation Science & Engineering, Nanjing Tech. University, Nanjing, Jiangsu 210009, China

Zheng-hua ZHOU
College of Transportation Science & Engineering, Nanjing Tech. University, Nanjing, Jiangsu 210009, China

Jie SU
College of Transportation Science & Engineering, Nanjing Tech. University, Nanjing, Jiangsu 210009, China

Xiao-jun LI
College of Architecture and Civil Engineering, Beijing University of Technology, Beijing 100124, China

See next page for additional authors

A constitutive model considering post-liquefaction deformation based on the logarithmic skeleton curve

Authors

Qing DONG, Zheng-hua ZHOU, Jie SU, Xiao-jun LI, and Bing HAO

Rock and Soil Mechanics 2021 42(7): 1903−1910 ISSN 1000−7598
https: //doi.org/10.16285/j.rsm.2019.6957 rocksoilmech.researchcommons.org/journal

A constitutive model considering post-liquefaction deformation based on the logarithmic skeleton curve

DONG Qing[1], ZHOU Zheng-hua[1], SU Jie[1], LI Xiao-jun[2], HAO Bing[1]

1. College of Transportation Science & Engineering, Nanjing Tech. University, Nanjing, Jiangsu 210009, China
2. College of Architecture and Civil Engineering, Beijing University of Technology, Beijing 100124, China

Abstract: Most of the constitutive model for liquefaction analysis cannot simulate the large post-liquefaction deformation of saturated sand, and there is little research on the nonlinear time-domain large deformation constitutive relationships suitable for seismic response analysis of saturated sand sites. In this paper, a feasible, simple and applicable large deformation constitutive model for time domain analysis is proposed through experimental analysis and theoretical research. The post-liquefaction stress-strain relationships of liquefied sand are obtained based on the undrained cyclic triaxial test data, then loading-reloading rules of large post-liquefaction deformation are proposed. Combined with the effective stress constitutive model based on logarithmic skeleton curve, a constitutive model that can quantitatively describe the large deformation of saturated sand liquefaction is proposed. According to the test results, the constitutive model can simulate small to large deformations from the pre-to post-liquefaction regime of sand. This constitutive model is also implemented to the program Soilresp1D for the dynamic response analysis of liquefiable soil sites. The results show that the time domain nonlinear large deformation unified constitutive model based on the logarithmic dynamic skeleton curve, effective stress-modified logarithmic dynamic skeleton constitutive model and liquefaction large deformation constitutive model can be directly applied to the dynamic response analysis of saturated sand.

Keywords: logarithmic skeleton curve; effective stress; liquefaction of saturated sand; loading-unloading rules; large deformation constitutive model

1 Introduction

The disasters induced by the liquefaction of saturated sand layer are mainly due to large deformation for liquefaction. Therefore, it is important to choose a suitable dynamic constitutive model for saturated sand when studying liquefaction. A large number of nonlinear or elastoplastic constitutive models have been proposed[1−2] for liquefaction analysis, including boundary surface models[3−5] and multi-surface models [6−7]. However, these models can only simulate the small deformation dynamic response of the soil layer during initial pre-liquefaction, and it is difficult to simulate the large deformation dynamic response of the liquefied sand layer under cyclic loading. Wang et al.[8], Wang et al. [9] and Wei et al.[10] based on the large deformation mechanism of saturated sand liquefaction proposed by Shmoto et al. [11], obtained the relevant liquefaction constitutive models, which are applicable to the large deformation dynamic response for sand liquefaction. But the mathematical constitutive model is complex, with many soil layer parameters, and the dynamic response analysis relies on finite element calculation software, so the calculation is cumbersome and time-consuming.

The selection of effective stress constitutive model before liquefaction is important for analyzing the dynamic response of saturated sand under large deformations. The reasonable pore pressure development model is the premise of studying the effective stress constitutive model of saturated sand. Chen et al.[12] proposed an incremental calculation model for pore pressure development of unevenly consolidated saturated sand suitable for horizontal sites according to the cyclic triaxial and shear test results. Based on the pore pressure development model, and combined with the time domain constitutive mode based on logarithmic skeleton curve [13], we have developed an effective stress constitutive model of pre-liquefaction saturated sand under strong earthquake. However, this constitutive model can only simulate the small deformation dynamic response of sand for pre-liquefaction, and cannot simulate the large deformation of saturated sand for post-liquefaction.

In view of the lack of a time domain constitutive model to simulate the large deformation of saturated sand for post-liquefaction. The aim of this study is try to develop a time domain constitutive model to simulate the large deformation of saturated sand for post-liquefaction by analyzing the stress−strain curves of pre-to post-liquefaction for saturated sand under the condition of undrained cyclic triaxial test. And then by

Received: 17 November 2019 Revised: 19 May 2021
This work was supported by the National Natural Science Foundation of China (U1839202) and the National Program on Key Basic Research Project of China (2017YFC1500400).
First author: DONG Qing, female, born in 1992, PhD candidate, majoring in rock and soil mechanics. E-mail: 2458810997@qq.com

combining with the time domain effective stress constitutive model, the whole response process of saturated sand for pre-to post-liquefaction under strong earthquake is described. For this purpose, undrained cyclic triaxial tests[13] have been carried out on the saturated Nanjing fine sand with a relative density of 45%. In the test, the effective confining pressure was 100 kPa, the cyclic stress ratio(CSR) was 0.3, and the loading frequency was 0.5 Hz. The stress−strain curves of pre-to post-liquefaction is shown in Fig.1, where Fig.1(c) and Fig.1(d) are derived from the decomposition of Fig.1(a). By comparing Figs.1(c) and (d), it can be seen that the upper half of the skeleton curve of saturated sand for pre-liquefaction is convex, and the upper half of the skeleton curve for post-liquefaction is concave, and both curves are antisymmetric. As shown in Fig.1(b), when the soil pore pressure ratio is close to 1, that is, when the effective stress of soil approaches 0, the soil liquefies, and the shear strain of liquefaction gradually increases with the increase of the number of cycles. The shear stress decreases in the early stage of liquefaction and then stabilizes. The shear modulus after liquefaction is consistent with the change trend before liquefaction, and there is a certain softening phenomenon, as the number of cycles increases. The variation trend of the shear modulus for post-liquefaction is consistent with that for pre-liquefaction, and there is softening phenomenon with the increase of the number of cycles. These limited descriptions of liquefaction large deformation tests need to be expressed by definite function expressions or mathematical models to realize the establishment of large deformation constitutive model of saturated sand for liquefaction.

In this study, combined with the large deformation stress−strain curve of the undrained cyclic triaxial test on saturated sand, the loading−unloading stress−strain curve is disassembled, and the loading−unloading rules are established. According to the rules, a time domain nonlinear large deformation mathematical model is proposed to describe the large deformation development of saturated sand post-liquefaction. This mathematical model can simulate the stress−strain response of saturated sand during the liquefaction process under cyclic loading, and can reasonably represent the development process of large deformation during liquefaction. Combined the logarithmic dynamic skeleton constitutive model and the effective stress constitutive model, an overlapping difference scheme is used to establish a time domain nonlinear dynamic response analysis method for a one-dimensional liquefiable site. The authors improved the self-developed program Soilresp1D, added effective stress constitutive model and liquefaction large deformation constitutive model, and realized the whole process numerical simulation of the time domain nonlinear dynamic response of a one-dimensional liquefiable site.

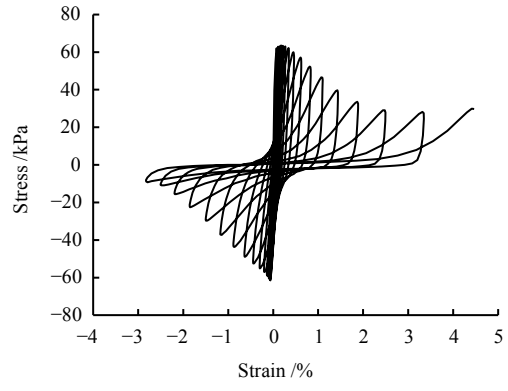

(a) Overall stress−strain curve

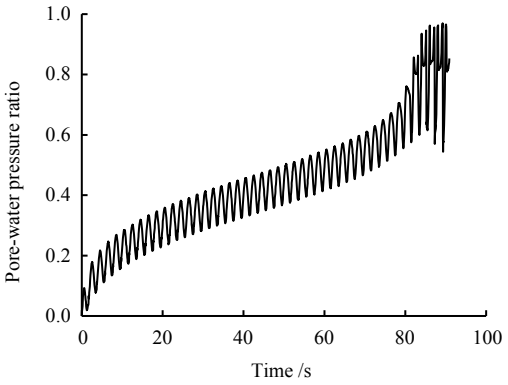

(b) Pore-water pressure variation of saturated fine sand under the undrained cyclic triaxial test

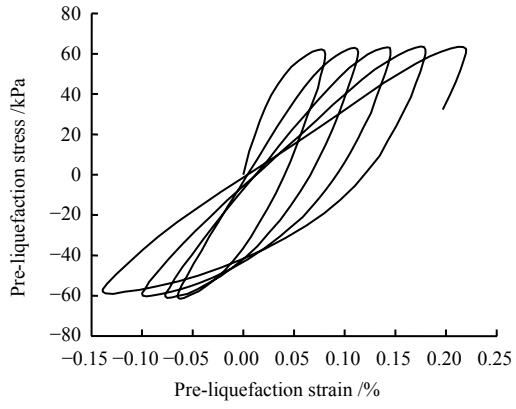

(c) Stress−strain curve before liquefaction

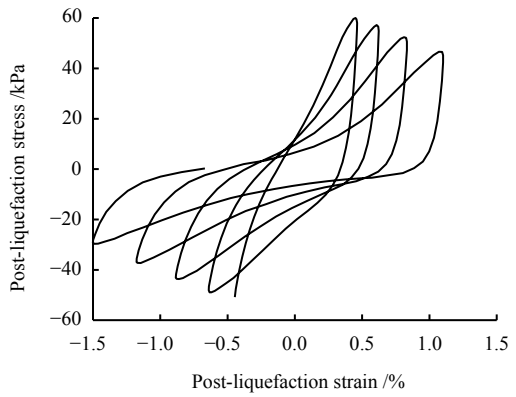

(d) Stress−strain curves of saturated sand after liquefaction

Fig. 1 Experimental results of saturated sand under undrained cyclic triaxial test

2 Loading−unloading rules

Under cyclic loading, the pore pressure of saturated sand increases with increasing number of cycles, causing soil softening. The modulus and shear strength of soil decrease with increasing pore water pressure. The stress−strain relationship of the soil for pre-liquefaction directly depends on the pore pressure. Liquefaction occurs when saturated sand reaches a state of zero effective stress. Then, the pore pressure no longer increases, the shear strength fails, the stress gradually decreases, and the strain gradually increases. As a result, the stress−strain curve differs from the shape prior to liquefaction. Therefore, this paper will simulate the stress−strain loading and unloading process of the sand for post-liquefaction. The expression of function and associated coefficients are determined to provide a constitutive model for solving the dynamic response of sand for post-liquefaction.

2.1 Basic function for stress−strain relationships of sand after liquefaction

The stress−strain loading and unloading process of saturated sand for post-liquefaction under the test conditions shown in Fig.1 are refined and analyzed. It can be disassembled into 4 stages as shown in Fig.2(a). *AB* section is forward loading, *BC* section is unloading 1, *CD* section is unloading 2, and *DA* section is reverse loading. The shapes of *BC* section and *AB* section are similar. The *DA* section is symmetric with *AB* section about the 0 point, the *CD* section is a straight line, and the curves of each section are connected by the control points (*A*, *B*, *C*, *D*). Figure 2(b) shows the two curves of the upper half of the loading hysteresis loop for soil pre-to post-liquefaction. It can be seen that the curves of *AB* section before and after liquefaction are symmetrical about the straight-line y–x=0. Then, the independent variable γ and the dependent variable τ in the stress−strain relationship $\tau = \gamma / (a + b\gamma)$ [14]of the hyperbolic model for pre-liquefaction are interchanged, and the basic functional formula of the stress−strain relationship of the post-liquefaction sand can be obtained:

$$\gamma = \frac{\tau}{a + b\tau} \tag{1}$$

where τ and γ are the shear stress and shear strain; a and b are the shear modulus and shear strength parameters of the soil.

After rearranging

$$\tau = \frac{\gamma}{1/a - \gamma b/a} = \frac{\gamma}{a_1 - b_1\gamma} \tag{2}$$

where a_1 is the initial tangent modulus of stress−strain for the post-liquefaction soil; b_1 is the test parameter. From Eq.(2), it can be seen that when the strain approaches a_1/b_1, τ tends to infinity, and a_1/b_1 is the asymptote of γ.

Figure 2(c) shows the fitting result of the test curve *AB* section through Eq. (2), and the fitting effect is excellent.

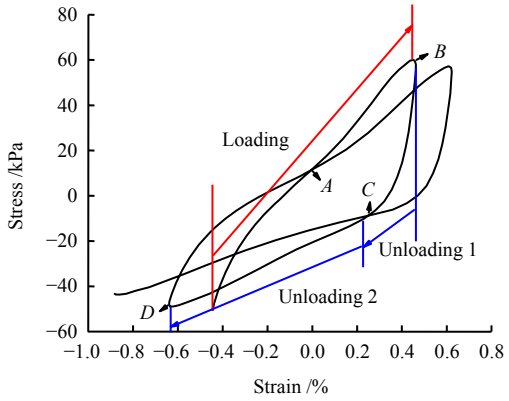

(a) Stress−strain disassembly diagram for first two cycles after liquefaction

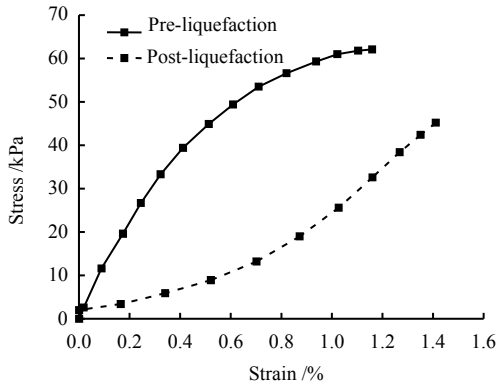

(b) Comparison of pre-to post-liquefaction main curves

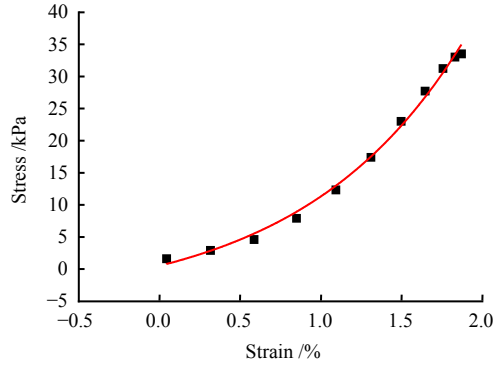

(c) Test curve fitting result

Fig. 2 Stress−strain relationships of liquefied sand

2.2 Large deformation loading−unloading rules

In each shearing cycle for post-liquefaction, the pore pressure of sand also fluctuates correspondingly, the effective stress fluctuates around 0, and the extreme value of pore pressure no longer increases. Therefore, the default pore pressure ratio of post-liquefaction is 1 in this paper. The stress−strain curve of the sand for post-liquefaction is analyzed according to the process of loading−unloading−reverse loading. The stress−strain relationship for post-liquefaction is calculated from the end of the reverse loading for the previous shear

cycle to the beginning of the positive loading for the new cycle. The control point of the stress−strain curve changes in each shear cycle. According to the undrained cyclic shear test curve shown in Fig.2 and the basic stress−strain Eq. (2), the five rules on large deformation loading-unloading are determined as follows:

(1) The stress−strain relationship of *AB* section in the positive loading process of the first cycle for post-liquefaction satisfies the basic function, where a_1 and b_1 are the values of *a* and *b* in the hysteresis process of the last loading and unloading before liquefaction. The stress and strain at point *A* $(\gamma_d,\ \tau_d)$ corresponding to the first loading step after positive loading are recorded.

(2) When the load reaches the turning point *B* $(\gamma_c,\ \tau_c)$, then it enters the unloading process. The unloading process is divided into the *BC* section and *CD* section. The stress−strain relationship of the *BC* section also conforms to the basic function. The undrained cyclic shear test results show that point *C* $(\gamma_{d1},\ \tau_{d1})$ is related to point *B*. The relationship between the two points is related to the degree of sand compaction.

(3) The unloading process of the *CD* section satisfies the linear function relationship.

(4) When unloading to the starting point *D* $(\gamma_c',\ \tau_c')$ of the reverse loading, record the coordinates of point *D*. The stress−strain curve at this stage also satisfies the basic function.

(5) When the stress−strain curve is loaded to point *A*, a new stress−strain cycle begins. The tangent modulus at the initial point *A* of this cycle is related to the properties of the soil and the number of cycles. The test results show that this curve and the *DA* curve are symmetrical about point *A*.

(6) The large deformation loading rules (2)−(5) are gradually cycled until the end of the dynamic loading.

In the above cyclic loading and unloading process, except the connection points *C* and a_1 of the two-stage unloading process, which need to be obtained by fitting the undrained cyclic shear test data after liquefaction, the remaining parameters b_1, b_2, and b_3 can be obtained through the turning point value in the stress−strain history. The variation of the parameter a_1 obtained by fitting the stress−strain curve of saturated Nanjing fine sand for post-liquefaction under different stress conditions with the number of cycles is shown in Fig.3. a_1 linearly decreases with the increase of the number of cycles, the reduction relation has nothing to do with the stress state of soil. Where, $a_{1,0}$ is the a_1 of the soil for pre-liquefaction, and $a_{1,N}$ is the a_1 of the soil when the number of cycles for post-liquefaction is *N*.

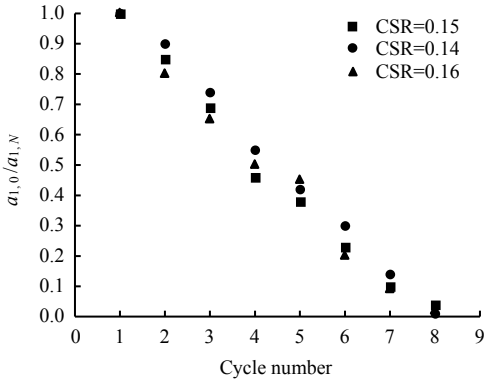

Fig. 3 Parameter change with number of cycles after liquefaction

3 Description of time domain nonlinear large deformation unified constitutive model

Based on the logarithmic dynamic skeleton model and the Chen's[12] pore pressure development model, combined with the above-mentioned large deformation constitutive model for post-liquefaction, a time domain nonlinear large deformation constitutive model is proposed and is applied to the time domain nonlinear dynamic response analysis of soil layers. This analysis method can completely simulate the stress−strain behavior and dynamic response of saturated sand for pre-to post-liquefaction.

3.1 Description of stress−strain relationships

The authors combine the concepts of "logarithmic skeleton curve" and "dynamic skeleton curve" to achieve a one-dimensional time domain dynamic nonlinear constitutive model based on logarithmic dynamic skeleton[14]. This constitutive model starts from the logarithmic skeleton curve shown in the following formula, and follows the "Masing's Law" and the basic assumptions of the logarithmic skeleton constitutive model (see literature [14] for details).

According to the definition of the logarithmic skeleton model, the functions of $f(\gamma)$ and $g(\gamma')$ are as follows:

$$f(\gamma)=\pm\ln(1\pm b\gamma/a)/b \tag{3}$$

$$g(\gamma')=\pm\ln\left(1\pm b'\gamma'/a'\right)/b' \tag{4}$$

where $f(\gamma)$ is the skeleton curve; $g(\gamma')$ is the dynamic skeleton curve; *a*, *b* can be obtained by fitting $G/G_0-\gamma$ test data; from the same initial modulus and extreme points of the skeleton curve and the dynamic skeleton curve, a' and b' can be calculated. When γ is a positive value, formulas (3) and (4) take "+"; when γ is a negative value, formulas (3) and (4) take "–".

Introducing the "damping ratio degradation coefficient" on the basis of logarithmic dynamic skeleton model, the time domain constitutive model of saturated sand for pre-liquefaction can be obtained as

$$\tau(r)=\begin{cases}\tau_{\mathrm{c}}+K(\gamma_0)\left[2g\left(\dfrac{\gamma-\gamma_{\mathrm{c}}}{2}\right)-G_{\mathrm{m}}\cdot\right.\\ \left.(\gamma-\gamma_{\mathrm{c}})\right]+G_{\mathrm{m}}(\gamma-\gamma_{\mathrm{c}}),\ |\gamma|\leqslant\gamma_{\mathrm{m}}\\ f(\gamma),\ |\gamma|>\gamma_{\mathrm{m}}\end{cases}\tag{5}$$

$$K(\gamma_0)=\frac{\pi b\gamma_0^2}{2\left(a^1+b^1\gamma_0\right)\left[(2a+b\gamma_0)-2b\gamma_0/\ln(1+b\gamma_0/a)\right]}\tag{6}$$

where $g\left(\dfrac{\gamma-\gamma_{\mathrm{c}}}{2}\right)$ is the dynamic skeleton curve; a^1 and b^1 are test parameters, which can be achieved by fitting the test data of damping ratio $\lambda-$strain γ; τ_{c} and γ_{c} are the stress and strain values corresponding to the last turning point of the stress−strain history; $G_{\mathrm{m}}=\dfrac{\pm\tau_{\mathrm{m}}-\tau_{\mathrm{c}}}{\pm\gamma_{\mathrm{m}}-\gamma_{\mathrm{c}}}$; τ_{m} and γ_{m} are the absolute values of the maximum turning point of historical stress−strain; $\gamma_0=\left|\dfrac{\pm\gamma_{\mathrm{m}}-\gamma_{\mathrm{c}}}{2}\right|$, when γ increases, the ± in the two equations is taken as +, when γ decreases, the ± in the two equations is taken as −; and $K(\gamma_0)$ is the damping ratio degradation coefficient. Its derivation process is reported in literature [14].

After saturated sand is subjected to cyclic loading, the pore pressure increment can be obtained through the introduction of the pore pressure increment model, and the pore pressure after cyclic loading is achieved through accumulation of the pore pressure increment, and the effective stress is calculated. When the effective stress is 0, the soil layer is considered to be liquefied. The stress−strain relationship of saturated sand after liquefaction no longer conforms to Eq. (5), but follows the aforementioned five rules on large deformation loading−unloading. Combining the rules and the undrained cyclic shear test data, the stress−strain constitutive relationship of saturated sand after liquefaction is derived as

$$\left.\begin{aligned}&\tau=\frac{\gamma-\gamma_{\mathrm{d}}}{a-b(\gamma-\gamma_{\mathrm{d}})}-\tau_{\mathrm{d}},n=1,\Delta\gamma\geqslant0,\gamma\geqslant\gamma_{\mathrm{d}}\\&\tau=\frac{\gamma-\gamma_{\mathrm{d1}}}{a_1-b_2(\gamma-\gamma_{\mathrm{d1}})}-\tau_{\mathrm{d1}},\Delta\gamma<0,\gamma\geqslant\gamma_{\mathrm{d1}}\\&\tau=\frac{\gamma-\gamma_{\mathrm{d1}}}{a_1}-\tau_{\mathrm{d1}},\Delta\gamma<0,\gamma<\gamma_{\mathrm{d1}}\\&\tau=\frac{\gamma-\gamma_{\mathrm{d}}}{a_1-b_3(\gamma-\gamma_{\mathrm{d}})}-\tau_{\mathrm{d}},\Delta\gamma\geqslant0,\gamma<\gamma_{\mathrm{d}}\\&\tau=\frac{\gamma-\gamma_{\mathrm{d}}}{a_1-b_1(\gamma-\gamma_{\mathrm{d}})}-\tau_{\mathrm{d}},n>1\Delta\gamma\geqslant0,\gamma\geqslant\gamma_{\mathrm{d}}\end{aligned}\right\}\tag{7}$$

in formulas:

$$\left.\begin{aligned}&b_2=\frac{a_1}{\gamma_{\mathrm{c}}-\gamma_{\mathrm{d1}}}-\frac{1}{\tau_{\mathrm{c}}-\tau_{\mathrm{d1}}}\\&b_3=\frac{a_1}{\gamma_{\mathrm{d}}-\gamma_{\mathrm{c}}'}+\frac{1}{(\tau_{\mathrm{c}}'-\tau_{\mathrm{d}})}\\&b_1=\frac{a_1}{-\gamma_{\mathrm{c}}'-\gamma_{\mathrm{d}}}-\frac{1}{(-\tau_{\mathrm{c}}'-\tau_{\mathrm{d}})}\end{aligned}\right\}\tag{8}$$

where n is the number of cycles after liquefaction; $(\gamma_{\mathrm{d}},\ \tau_{\mathrm{d}})$ is the strain and stress corresponding to the forward loading point A in each cycle; $(\gamma_{\mathrm{c}},\ \tau_{\mathrm{c}})$ and $(\gamma_{\mathrm{c}}',\ \tau_{\mathrm{c}}')$ are the strain and stress corresponding to the turning points B and D; $(\gamma_{\mathrm{d1}},\ \tau_{\mathrm{d1}})$ is the strain and stress of the connecting point of the two unloading processes.

Equations (5) and (7) constitute the nonlinear dynamic constitutive model of saturated sand for pre-to post-liquefaction, with fewer parameters that can be obtained from the undrained cyclic shear test data. The unified nonlinear large deformation constitutive model can be directly applied to analyze the large deformation dynamic response of saturated sand for post-liquefaction.

3.2 Pore pressure increment model

Before the liquefaction of the saturated sand, the pore pressure increment model for each loading cycle process adopts the pore pressure increment model proposed by Chen et al.[12], which is suitable for horizontal sites, as shown in the following:

$$\left.\begin{aligned}&u_0^*=0\\&U_N=\frac{\Delta u_N^*}{1-u_{N-1}^*}=\frac{c_{1,0}}{\sqrt{N_{\mathrm{ep}}}}\left(\frac{\tau_N}{\bar{\sigma}_{N-1}}\right)^{A_{4,0}}\cdot\\&\left[1-c_{1,\mathrm{a}}\left(K_{\mathrm{c}}-1\right)^{c_{1,\mathrm{b}}}\right],N=1,2,3,\ldots\\&u_N^*=u_{N-1}^*+U_N\left(1-u_{N-1}^*\right)\\&N_{\mathrm{ep}}=\sum_{i=1}^{N}\left[\frac{\tau_i}{\tau_N}\right]^{\alpha}\end{aligned}\right\}\tag{9}$$

where u_0^* is the initial pore pressure ratio; $\Delta u_N^*=\Delta u_N/\bar{\sigma}_0$, Δu_N is the pore pressure increment in the Nth stress cycle, $\bar{\sigma}_0$ is the initial effective confining stress; $\Delta u_{N-1}^*=\Delta u_{N-1}/\bar{\sigma}_0$, u_{N-1} is the pore pressure in the N–1th stress cycle; $c_{1,0}$, $c_{1,\mathrm{a}}$, $c_{1,\mathrm{b}}$, and $A_{4,0}$ are test parameters, which are related to the degree of compaction; K_{c} is the consolidation ratio; N_{ep} is the number of equivalent stress loading; τ_i is the amplitude of the ith cyclic shear stress ($1\leqslant i\leqslant N$); τ_N is the amplitude of the Nth cyclic shear stress; and α is the material parameter. The values of related parameters in the formula are reported in the literature [12], which are not repeated here.

3.3 Modification of shear modulus and shear strength

The influence of rise of pore pressure on the dynamic response of saturated sand is reflected by the modification for shear modulus and shear strength. The shear modulus and shear strength of saturated sand decrease with increasing pore pressure. After a stress cycle, the shear modulus and shear strength are corrected according to the following:

$$\left.\begin{aligned}\bar{\sigma}_{0,N} &= \bar{\sigma}_{0,N-1} - \Delta u_N \\ G_{\max,N} &= G_{\max,N-1}\left(\frac{\bar{\sigma}_{0,N}}{\bar{\sigma}_{0,N-1}}\right)^{C_3} \\ \tau_{y,N} &= \tau_{y,N-1}\left(\frac{\bar{\sigma}_{0,N}}{\bar{\sigma}_{0,N-1}}\right)^{B_3}\end{aligned}\right\} \quad (10)$$

where $G_{\max,N}$, $\tau_{y,N}$ and $\bar{\sigma}_{0,N}$ are the shear modulus, shear strength and effective stress of the soil after N–1th stress cycles; C_3 and B_3 are test parameters, which can be found in literature [15].

3.4 Numerical simulation of time domain dynamic response for saturated sand

On the basis of the time domain nonlinear dynamic response analysis method of soil layers based on overlapping grids[16−17], the large deformation constitutive model proposed in this paper is introduced for saturated sand for pre-to post-liquefaction. A time domain analysis method is developed to simulate the dynamic response of saturated sand for pre-to post-liquefaction. This method has a wide range of applications and can be used to calculate and analyze the dynamic response of sites with or without saturated sand.

When the relevant soil parameters are known, combined with Eq.(5) and Eq.(7), the time-domain nonlinear dynamic response analysis method of soil layers based on overlapping grids can be used to calculate the dynamic response of arbitrary section at any time during the entire liquefaction process of the saturated sand layer. The implementation program is a self-developed program Soilresp1D, a time-domain nonlinear dynamic response analysis program that introduces a unified constitutive relationship of saturated sand with large deformation. Fig.4 is a flowchart of the detailed implementation of the Soilresp1D. In the figure, Δt is the discrete time interval, h_n is the thickness of the discrete soil layer, N is the number of discrete soil layers, i is the time step, and j is the serial number of soil layer.

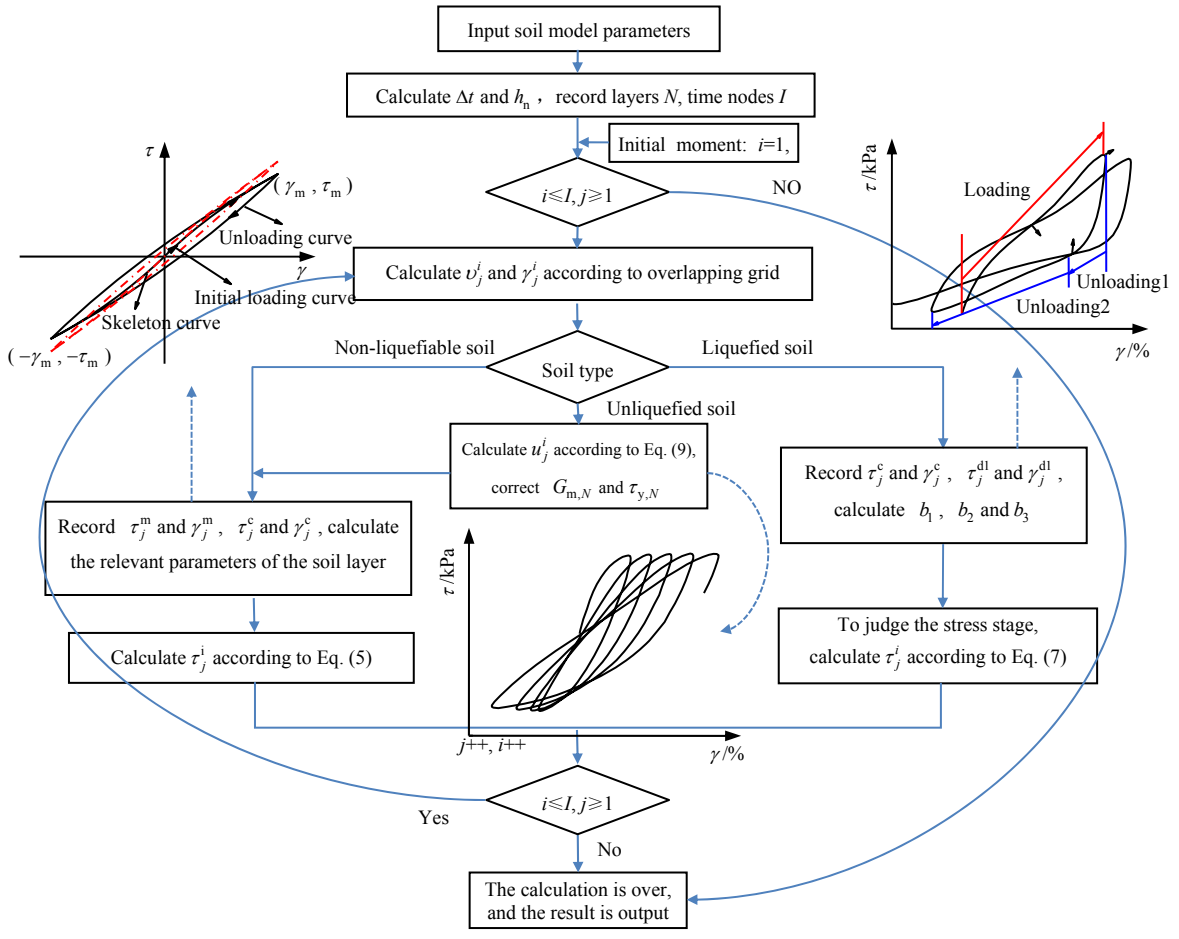

Fig.4 Algorithm implementation flowchart

4 Preliminary realization of time domain constitutive model considering liquefaction large deformation

The dynamic response of a saturated sand site under a sine wave with an input period of 1s was analyzed as an example. The time domain constitutive model that can be considered for liquefaction and large deformation is initially implemented in Soilresp1D, and its feasibility and reliability are tested.

The analyzed site includes clay layer, saturated sand layer and underlying bedrock. The total thickness is 32 m. The mechanical parameters of rock and soil layers are shown in Table 1. The relationship between soil shear wave velocity v_s and depth z is $v_s = 120 + 3.7z$. In order to compare with the test results, an undrained cyclic triaxial test has been carried out on the saturated loose fine sand. In the test, the effective confining pressure was 100 kPa, the cyclic stress ratio is 0.13, and the loading frequency is 1 Hz. According to the calculation accuracy requirements of the time-domain nonlinear dynamic response analysis method of soil layers based on overlapping grids, the discrete step Δz along the depth of the site was determined to be 1m, and the 7th, 8th, and 9th layers from top to bottom were saturated loose fine sandy soil layer. The input sine wave had a duration of 48 s, a period of 1 s, and an amplitude of 0.70 m/s^2. According to the stability requirements of the time-domain nonlinear dynamic response analysis method, the time step was determined to be 0.002 5 s. In the analysis model, the stress−strain relationship of clay was based on the logarithmic dynamic skeleton constitutive model, and its constitutive parameters were determined based on the test data of $G / G_0 - \gamma$ and $\lambda - \gamma$, as shown in Table 2. The stress−strain relationship of bedrock adopted linear elastic constitutive, and the shear modulus was taken as a constant. The stress−strain relationship of the saturated fine sand before liquefaction adopted the logarithmic dynamic skeleton constitutive model based on the effective stress correction. After each stress cycle, the pore pressure of the saturated fine sand can be obtained from Eq.(9). The effective stress was calculated according to Eq. (10). $G_{\max,N}$ and $\tau_{y,N}$ were corrected accordingly. When the saturated fine sand reaches the effective stress state of 0, the stress−strain relationship adopted the large deformation constitutive model, and the corresponding constitutive parameters are shown in Table 2.

Table 1 Site calculation model

Soil layer	Depth /m	Thickness /m	Shear wave velocity /(m • s^{-1})	Density /(kg • m^{-3})
Clay	6	6	120.0～142.2	1.95×10^3
Fine sand	9	3	142.2～153.3	1.49×10^3
Clay	30	21	153.3～231.0	1.95×10^3
Bedrock	32	2	511.0	2.65×10^3

Table 2 Model calculation parameters

Soil type	a_1an	γ_d / γ_c	τ_d / τ_c	b/a	$a^1 / 10^{-3}$	b^1	$c_{1,0}$	$c_{1,a}$	$c_{1,b}$	$A_{4,0}$	C_3	B_3
Fine sand	0.34	0.75	0.11	1 934	2.24	5.2	33.71	0.38	0.56	2.61	0.49	1.0
Clay				1 160	0.82	5.9						

The comparison between the test results and the numerical simulation results is shown in Fig.5. Fig.5(a) shows that the pore pressure ratio of the 7th layer of sand is 1 at 16.5 s, and sand starts to liquefy; no liquefaction occurs in the 8th and 9th layers, and the pore pressure ratio tended to be flat after the 7th layer liquefaction. In Fig.5(b), the peak value of ground acceleration is 1.24 m/s^2, the amplification factor is 1.77, and the ground acceleration is significantly attenuated after liquefaction. The stress of 7th sand layer is consistent with that of the test sand. Comparison between the numerical results and test results of stress−strain for 7th sand layer is presented in Figs.5(c) and 5(d). Fig.5(c) illustrates that the saturated fine sand under dynamic cycle is in nonlinear stress−strain state; the numerical results are similar to the test results; the shear modulus decreases with the increasing number of cycles; and the stress−strain curve tends to be flat. The large deformation stress−strain hysteresis loop for post-liquefaction is plotted in Fig.5(d), and its changing trend is similar to the test results. As the number of cycles increases, the stress corresponding to the turning point of the transition from the positive loading to the first stage unloading gradually decreases, and the strain gradually increases. This stress−strain characteristic follows the large deformation loading−unloading rules determined in this paper. The results of site dynamic response analysis show that the ground acceleration time-history amplitude before liquefaction is significantly larger than that after liquefaction when considering large deformation of liquefaction. It can be seen that the liquefaction of saturated sand has a significant damping effect on site dynamic response. This feature is consistent with some on-site observations of earthquakes.

The results of dynamic response analysis of saturated sandy soil show that it is feasible to apply the time domain nonlinear large deformation constitutive model based on logarithmic dynamic skeleton constitutive, the effective stress modified logarithmic dynamic skeleton constitutive and the liquefaction large deformation constitutive to the dynamic response analysis of saturated sandy soil, and the calculation result is reliable.

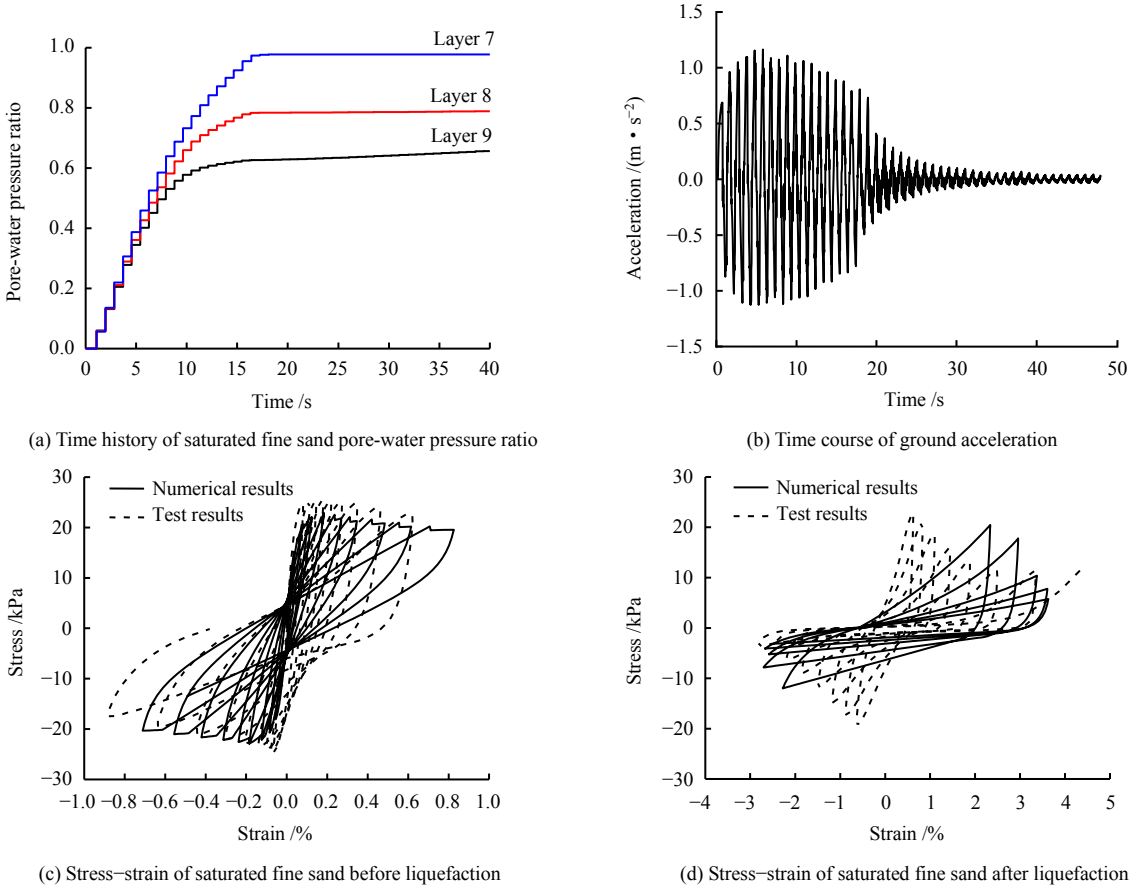

(a) Time history of saturated fine sand pore-water pressure ratio

(b) Time course of ground acceleration

(c) Stress−strain of saturated fine sand before liquefaction

(d) Stress−strain of saturated fine sand after liquefaction

Fig. 5 Comparison of the calculated and experimental results for seismic response of the site under input sine wave

5 Conclusions

(1) Based on the stress−strain curve of triaxial test of saturated sand with undrained cyclic loading, 4 loading−unloading stages of large deformation after liquefaction of saturated sand are defined, and 5 loading−unloading rules are determined.

(2) The basic function is determined according to the large deformation loading−unloading rules after saturated sand liquefaction and the stress−strain change law of each section. The method for determining the corresponding parameters is given combining the test data,

(3) The large deformation constitutive model of liquefied saturated sand is introduced into Soilresp1D, a time-domain nonlinear dynamic response analysis program developed by the authors. The dynamic response analysis of liquefaction large deformation of saturated sand sites is implemented.

(4) The simulation results of the dynamic response for saturated sandy soil site are similar to the test results. It suggests that liquefaction has a seismic mitigation effect on the dynamic response of the site.

It is worth pointing out that the dynamic response analysis method of saturated sand soil sites proposed in this paper is currently only verified by the dynamic response under symmetric cyclic loads, and the applicability to asymmetric seismic loads needs to be further verified by experiments.

References

[1] MARTIN G R, FINN W D L, SEED H B. Fundamentals of liquefaction under cyclic loading[J]. Journal of the Geotechnical Engineering Division, ASCE, 1975, 101(5): 423−438.

[2] FINN W D L. State-of-the-art of geotechnical earthquake engineering practice[J]. Soil Dynamics and Earthquake Engineering, 2000, (20): 1−15.

[3] WANG Z L, DAFALIAS Y F, SHEN C K. Bounding surface hyp-oplasticity model for sand[J]. Journal of Engineering Mechanics, 1990, 116(5): 983−1001.

[4] PAPADIMITRIOU A G, BOUCKOVALAS G D,

DAFALIAS Y F. Plasticity model for sand under small and large cyclic strains[J]. Journal of Geotechnical and Geoenvironmental Engineering, 2001, 127(11): 973−983.

[5] DAFALIAS Y F, MANZARI M T. Simple plasticity sand model accounting for fabric change effects[J]. Journal of Engineering Mechanics, 2004, 130(6): 622−634.

[6] PREVOST J H. A simple plasticity theory for frictional cohesionless soils[J]. Soil Dynamics and Earthquake Engineering, 1985, 4(1): 9−17.

[7] YANG Z, ELGAMAL A, PARRA E. Computational model for cyclic mobility and associated shear deformation[J]. Journal of Geotechnical and Geoenvironmental Engineering, 2003, 129(12): 1119−1127.

[8] WANG Gang, ZHANG Jian-min, WANG Rui. A cyclic elasto-plastic constitutive model for evaluating large liquefaction induced deformation of sand[J]. Chinese Journal of Geotechnical Engineering, 2007, 29(1): 51−59.

[9] WANG Rui, ZHANG Jian-min, WANG Gang. A cyclic elasto-plastic constitutive model for evaluating large liquefaction induced deformation of sand[J]. China Earthquake Engineering Journal, 2013, 35(1): 91−97.

[10] WEI Xing, ZHANG Zhao, WANG Gang, et al. DEM study of mechanism of large post-liquefaction deformation of saturated sand[J]. Rock and Soil Mechanics, 2019, 40(4): 1596−1602.

[11] SHAMOTO Y, ZHANG J M, GOTO S. Mechanism of large post-liquefaction deformation in saturated sands[J]. Soils and Foundations, 1997, 37(2): 71−80.

[12] CHEN Long-wei, YUAN Xiao-ming, SUN Rui. An incremental pore-water pressure buildup model for horizontal soil strata[J]. Journal of Basic Science and Engineering, 2010, 18(2): 190−198.

[13] MA Wei-jia, CHEN Guo-xing, WU Qi. Experimental study on liquefaction resistance of coral sand under complex loading conditions[J]. Rock and Soil Mechanics, 2020, 312(2): 179−186.

[14] DONG Qing, SU Jie, ZHOU Zheng-hua. The time domain constitutive based on logarithmic skeleton curve and its application in seismic response calculation, 2020, 42(8): 1491−1498.

[15] MASING G, Eigenspannungen und Verfestigungbeim Messing[C]//Proceedings of Second International Congress of Applied Mechanics. [S. l.]: [s. n.], 1926: 332−335.

[16] FENG Wang-ling, SHI Zhao-ji. Method of pore water pressure analysis for discrimination of liquefaction potential of horizontal layer[J]. Earthquake Resistant Engineering, 1988(4): 30−34.

[17] LIAO Zhen-peng. Introduction to wave motion theories in engineering[M]. Beijing: Science Press, 2002.